Journal of the European Ceramic Society 18 (1998) 113–122

PII: S0955-2219(97)00091-5
0955-2219/98/$19.00 + 0.00

Ageing Effects of Electrodes in Ceramic Fuel Cells

Vincenzo Antonucci,[a] Esterina Modica,[a] Giuseppe Monforte,[a] Antonino S. Aricò[a] and Pier Luigi Antonucci[b]

[a]Institute C.N.R.-T.A.E. for Transformation and Storage of Energy, via Salita S. Lucia sopra Contesse 39, 9826 S. Lucia, Messina, Italy
[b]University of Reggio Calabria, Faculty of Engineering, Institute of Chemistry, via E. Cuzzocrea 48, 89100 Reggio Calabria, Italy

(Received 18 November 1996; accepted 27 February 1997)

Abstract

A physico-chemical characterization of aged electrodes of a 150 W solid oxide fuel cell (SOFC) tubular stack is presented. X-ray diffraction and electron microscopy analyses showed that significant chemical and morphological changes occurred in both anodic and cathodic components after 3000 h operation. Depletion of ceria at the anode side with operation time caused a change in selectivity of the methane oxidation reaction, leading to a significant increase of the deep oxidation products in the catalytic step preceding the electrochemical reaction. This determined both OCV drop and performance decay. Moreover, prolonged operation resulted in a narrowing of the three-phase reaction zones at the electrode–electrolyte interface. © *1997 Elsevier Science Limited.*

1 Introduction

Solid oxide fuel cells (SOFCs) have undergone strong development in the last few years with the attainment of good performance and endurance, especially for stacks in tubular configuration; thus, efforts are continuing to further develop this highly efficient power generation system in order to speed up the demonstration of this technology on a commercial scale.

SOFCs have several distinct advantages with respect to other types of fuel cells, the most relevant of which are the invariability of the electrolyte and the possibility of using different kinds of fuels with sufficiently rapid reaction kinetics. On the other hand, the very stringent requirements of materials have represented the most critical issues for the acceptability of this technology worldwide. The specific materials problems appear to be numerous and diverse, and the progress toward their solution appears quite complex, as it involves many interdisciplinary aspects related to high temperature chemistry, electrochemistry, ceramics, engineering design and manufacturing.[1–5] The challenge is the development of suitable materials able to sustain adequate electrocatalytic activity without significant performance losses for tens of thousand of hours. The actual technology is still far away from this target, therefore many scientific efforts are addressed to the characterization of materials, components and complete cells to assess the physico-chemical and electrocatalytic properties of variously sized stacks under different conditions.

In this framework, a 150 W, 16-cell tubular stack was previously tested in a 3000 h endurance run; the stack was fuelled with methane, partially oxidized to synthesis gas, directly into the anodic compartment of the cell, to evaluate the practical reliability of the partial oxidation route as an alternative to the most generally adopted steam reforming process. A largely steady response was observed during the whole test, with the achievement of the target power;[6–8] only during the last hundreds hours of operation did the stack show a progressive decrease in electrochemical performance. After conclusion of the test, the stack was disassembled, in order to make a diagnosis of the observed performance loss, and the electrochemical activity of each cell was investigated. Furthermore, a careful examination of the single cells excluded the occurrence of short circuit phenomena or reactants leakage. Thus, two cells of the stack were selected on the basis of their performance and compared with a reference cell which was not previously used for electrochemical tests. No substantial changes were detected, by physico-chemical

and electrochemical investigations, in the electrolyte layer of the two selected aged cells with respect to the reference. Thus, an extensive characterization of the electrodes was made in order to determine the chemical and morphological modifications which occurred as a result of the endurance test: the paper presents the most interesting results of this evaluation.

2 Experimental

2.1 The stack

The fuel cell stack prototype was constituted by 16 tubular single cells electrically connected in series (Fig. 1) with coflow feed of gases which resulted in a compact geometry of the system. The single cell was self-supporting, since the ceramic tube acted as support for the deposited electrode; each tube had a thickness of 0·3 mm and it was closed at its lower edge. Relevant cell parameters were: length = 210 mm; diameter = 10 mm; operating area = 62·5 cm^2.

The electrolyte material was an Yttria-Scandia Stabilized Zirconia (YSSZ; $ZrO_2 = 90\%$; $Sc_2O_3 = 6\%$; $Y_2O_3 = 4\%$). Anode ($Pt–CeO_2$) and cathode ($Pt–PrO_2$) layers (thickness = 300 μm) were deposited by slurry painting onto the outer and inner part of the ceramic tube, respectively. The Pt-containing slurry was constituted by the powdered metal mixed with an organic dispersing agent; the subsequent heat treatment in inert atmosphere at 1200°C allowed the removal of the organic matter and the achievement of a strongly adhering, highly porous Pt layer. After cooling, deposition of the mixed conductors (CeO_2 at the anode, PrO_2 at the cathode) was carried out by impregnation and successive heat treatment (800–1000°C) of organic solutions of proper salt precursors. The two-step deposition was needed to avoid undesired structural modifications of the oxides, in the presence of Pt, at T > 1000°C. The presence of CeO_2 and PrO_2 mixed conductors in the electrode formulation was necessary in order to increase the extent of the three-phase reaction zone at both anode and cathode sides, respectively; an intimate contact between the electrode surface and the electrolyte would decrease the interfacial resistances associated with the ionic and electronic transfer during the elementary reaction steps. At the same time, $Pt–CeO_2$ is known to be an effective and selective catalyst for methane partial oxidation to synthesis gas.[9,10]

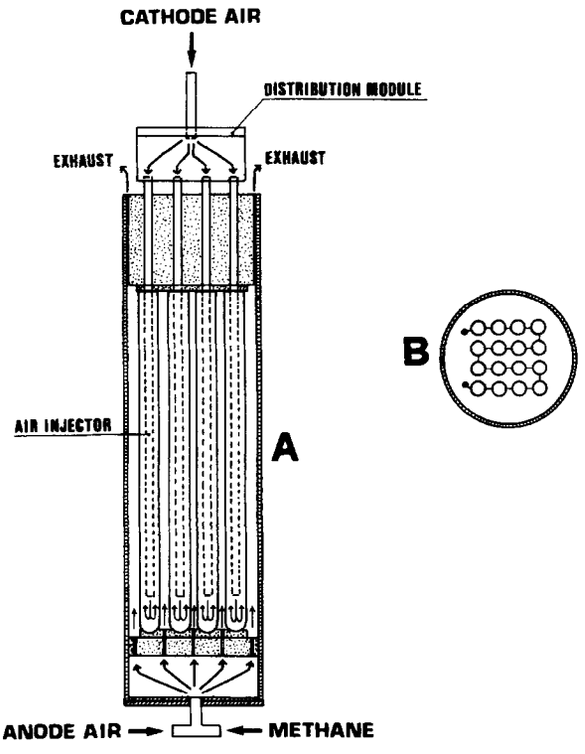

Fig. 1. Schematic view ofthe SOFC stack. (A) front, (B) top.

Anode feed inlets were located in a lateral position on the lower part of the stack; mixing of the gases occurs in the tube portion immediately preceding the electrochemical section. The cathodic air inlet was located in the middle position of the upper panel of the stack, and successively divided into sixteen paths through a cubic stainless steel distribution module including sixteen quartz air injectors.

Monitoring and manipulation of the operational parameters of the stack and single cells was achieved by the presence of proper control and regulation devices; a PC-interfaced data logger allowed data handling during performance and life-time tests under different operational conditions.

2.2 Materials characterization

XRD analysis was carried out with a Philips X-Pert diffractometer using a Cu Kα source operating at 40 kV and 30 mA. The X-ray diffraction patterns were collected at a scan rate of 2° two-theta min^{-1}. The spectral contribution from Cu Kα_2 was subtracted by a software correction algorithm. Diffraction peaks were attributed according to the Joint Committee on Powder Diffraction Standard (JCPDS) cards.

The mean particle size of Pt and CeO_2 was determined from the broadening of the (111) reflection of Pt and CeO_2 cubic structures. Peak profiles were obtained by a non-linear least-square fitting of the α_2-corrected data by using the Marquardt algorithm. The measured full width at half maximum (FWHM) values were corrected for the instrumental broadening by using the Warren formula.

Transmission electron microscopy (TEM) analysis was performed with an apparatus (Philips CM 12) equipped with super-twin objective lens, working at 120 kV accelerating voltage. The ultimate spatial resolution of the instrument was 2Å. Specimens were prepared by grinding the electrodes and ultrasonically suspending the particles in alcohol. Drops of the obtained suspension were deposited on a standard Cu grid covered with carbon film or onto a holey carbon grid and allowed to dry before being inserted into the microscope.

Morphology of the cell components was investigated with a Philips XL20 scanning electron microscope (SEM), equipped with a LaB_6 filament, working at an accelerating voltage of 20 kV. Chemical composition was determined by an energy dispersive X-ray microanalytic unit equipped with an ultrathin Be window.

3 The Partial Oxidation Reaction

The partial oxidation (oxyreforming) of methane to synthesis gas represents an alternative route to steam reforming for the direct utilization of natural gas in SOFCs. The reaction is slightly exothermic:

$$CH_4 + 1/2O_2 \rightarrow 2H_2 + CO \qquad \Delta H^\circ_{298} = -35 \cdot 6\ kJ\ mole^{-1} \tag{1}$$

and occurs under fuel-rich conditions ($CH_4/O_2 \cong 2$). The reaction involves an instant combustion of a fraction (~25%) of the methane feed:

$$CH_4 + 2O_2 \rightarrow CO_2 + 2H_2O \qquad \Delta H^\circ_{298} = -886 \cdot 16\ kJ\ mole^{-1} \tag{2}$$

with a complete consumption of the stoichiometrically limited oxygen.

The remaining quantity of CH_4 is reformed by both H_2O and CO_2, produced in the first step, according to the reactions:

$$CH_4 + H_2O \leftrightarrow CO + 3H_2 \qquad \Delta H^\circ_{298} = 226\ kJ\ mole^{-1} \tag{3}$$

$$CH_4 + CO_2 \leftrightarrow 2CO + 2H_2 \qquad \Delta H^\circ_{298} = 261\ kJ\ mole^{-1} \tag{4}$$

$$CO + H_2O \leftrightarrow CO_2 + H_2 \qquad \Delta H^\circ_{298} = -41 \cdot 19\ kJ\ mole^{-1} \tag{5}$$

As temperature is increased, the endothermic reactions (3) and (4) are favoured, and carbon monoxide and hydrogen become the main products.

4 Results and Discussion

Figure 2(a) shows typical I-V, I-W curves of the stack, denoting the attainment of the target power in absence of bad-functioning causes, under the following conditions: T = 950°C; O_2/CH_4 molar ratio = 0·5 (stoichiometric); CH_4 = 0·84 1 min^{-1}; anode air = 2·0 1min^{-1}; cathode air = 12·0 1 min^{-1}.

The stack performance after 3000 h operation is shown in Fig. 2(b), under the same conditions. An evident performance loss is observed, with the attainment of only about one third of the nominal power. As outlined in the introduction, two single cells, representative of the behaviour of the stack, were selected for the electrochemical and physicochemical characterization. Their I-V and I-W curves are presented in Fig. 3(a) and (b), respectively. A typical resistive behaviour was observed for the polarization curves in Fig. 3(a). A lowering of the electrical power output was observed for the

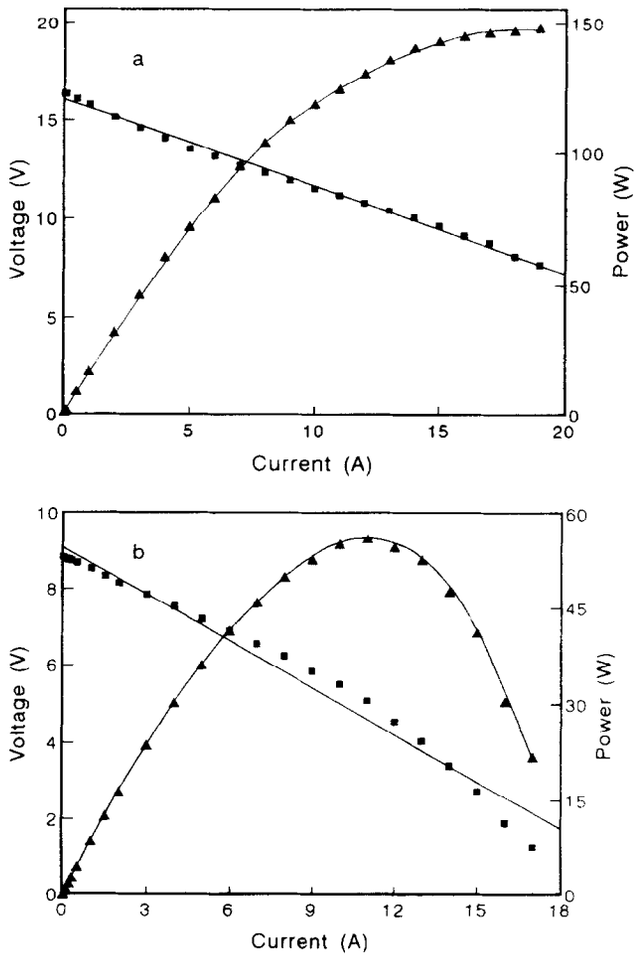

Fig. 2. Polarization (■) and power output curves (▲) of the stack: (a) nominal, (b) aged.

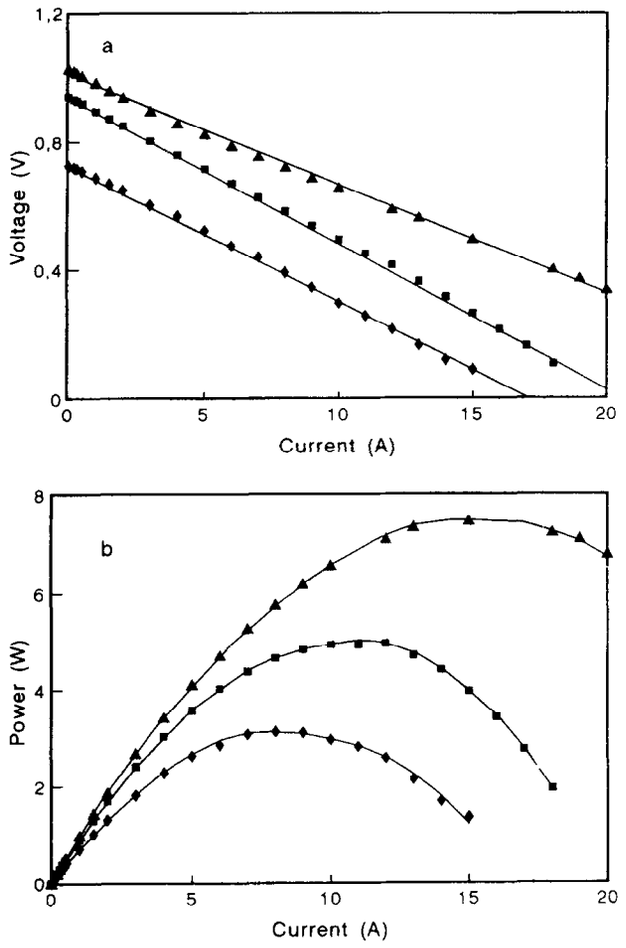

Fig. 3. Polarization (a) and power output, (b) curves of single cells; (▲) cell 0, (■) cell 6, (◆) cell 3.

aged cells with respect to the reference, as resulting from a significant decrease of open circuit voltage (OCV) and a slight increase of uncompensated resistance.

4.1 Anodes

Figure 4 shows the X-ray diffractograms of the anodes in the cells under examination. The typical reflections of platinum (JCPDS card no. 40802) and cerium oxide (JCPDS card no. 431002) are present in the three samples examined. A progressive decrease of the ratio between the integrated area intensities of CeO_2 (1,1,1) and Pt (1,1,1) peaks was observed, accounting for a relevant depletion of CeO_2 in the aged cells. The intensity scale for cell 3 was amplified in order to highlight the peaks related to secondary phases. A peculiarity of the reference cell is represented by a reflection ($2\theta = 56{\cdot}9°$) attributed to cubic $Ce_2Zr_2O_7$ (JCPDS card no. 8-221); this peak is still visible in the diffractogram of cell 6, whereas it completely disappears in cell 3 (Fig. 5). This evidence is interpreted in terms of progressive deterioration of the intimate electrolyte–anode interaction, previously achieved in the activation step of the anode layer. Another relevant phenomenon in the used anodes is the increase of a peak at $2\theta = 31{\cdot}4°$ related to a Pt–Ce alloy (JCPDS card no. 19-295); this effect is probably due to a progressive reduction of ceria in the reaction environment with subsequent charge transfer to Pt. In this regard, some evidence derived from XRD results is confirmed by the EDX analysis of the three anodes under examination [see Fig. 6(a)–(c)]; the Pt–Ce atomic ratio of cells 6 and 3 results sensibly higher than in the reference, passing from 0·59 for this latter to ~ 1 for the run cells. This significant depletion in cerium oxide on the electrode surface, together with formation of the Pt–Ce alloy, can in part explain the lower performance of cells 6 and 3 with respect to the reference, the so-altered catalyst composition appears to be less effective in promoting the methane conversion, as previously reported.[9,10] The redox behaviour of ceria is of fundamental importance in the reaction path, as follows:[10]

$$CeO_2 + nCH_4 \rightarrow CeO_{2-n} + nCO + 2nH_2 \qquad (6)$$

$$CeO_{2-n} + nCO_2 \rightarrow CeO_2 + nCO \qquad (7)$$

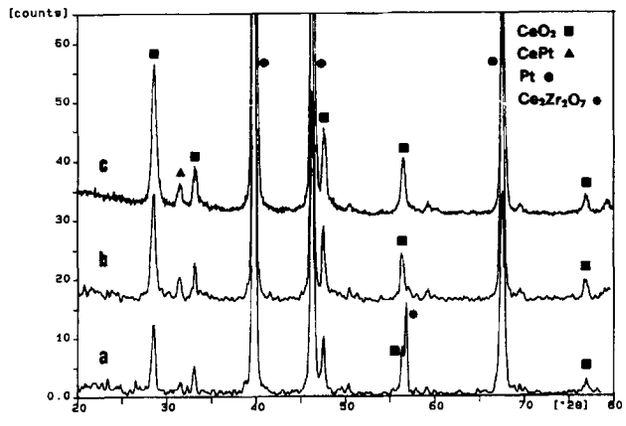

Fig. 4. XRD patterns of the anode layers: (a) cell 0, (b) cell 6, (c) cell 3.

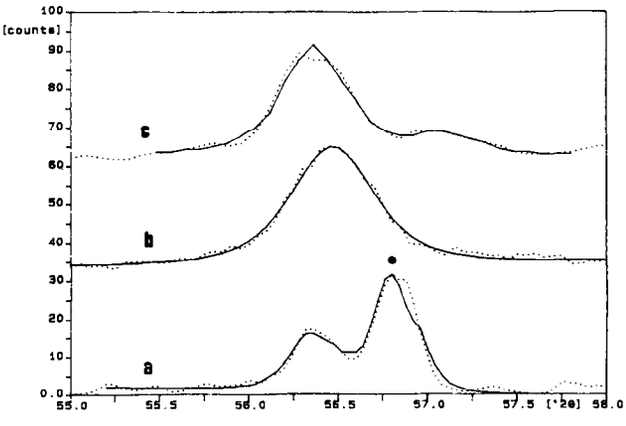

Fig. 5. X-ray profiles of (311) and (622) reflections of CeO_2 and $Ce_2Zr_2O_7$ phases in the anodes: (a) cell 0, (b) cell 6, (c) cell 3.

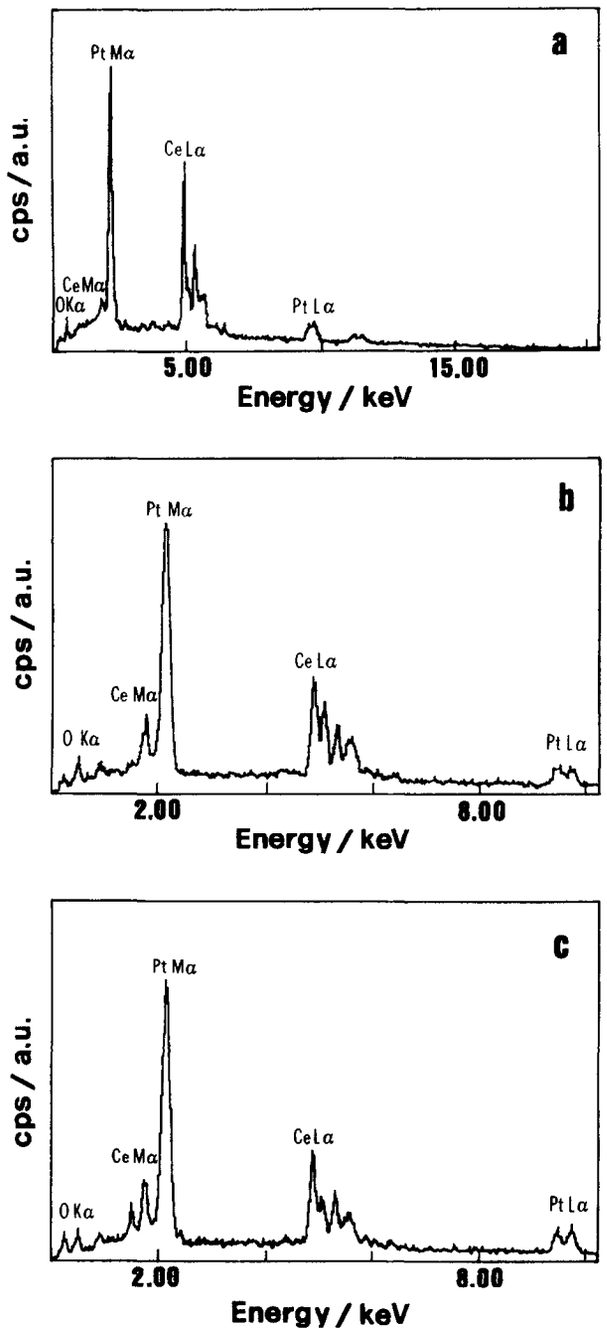

Fig. 6. EDX spectra of the anode layers: (a) cell 0, (b) cell 6, (c) cell 3.

Thus, depletion of ceria from the anode catalyst and the concurrent presence of Pt–Ce alloy gives rise to a Pt-rich phase which is known to be a total oxidation catalyst;[11] likewise, it is known that the addition of CeO_2 to Pt significantly increases CO and H_2 formation in the methane oxidation.[10] Accordingly, the selectivity of the reaction substantially changes towards the formation of CO_2 and H_2O as deep oxidation products which are not electrochemically active.

The other relevant effect which can be envisaged as a result of surface modifications induced by stack operation is attributable to a decrease in the extent of the three-phase reaction zone, probably due to the observed ceria depletion. As is well known,[12–14] stack performance is strongly depressed on account of a narrowing in the region where the electrode, electrolyte and gas phase intersect to accomplish the whole reactive process. Generally, the electrode surface should possess high electrical conductivity with ionic–electronic contributions, in order to reduce the internal resistance of the cell and enhance, at the same time, charge transfer and gas adsorption; this results in an increase of the electrode–electrolyte interface region, with consequent lower polarization. Since ceria is a mixed ionic-electronic conductor, its depletion at the electrode surface also plays a negative role for what concerns the missed 'spreading' of the electrode reaction zone around the triple contact point, with the consequent decrease in reaction rate.

Concurrent evidence associated with the above is the detection of an electron-conducting Pt–Ce phase in the used anodes, as previously anticipated. In this way, the above-described positive effects exerted by the presence of ceria at the three-phase zone are weakened. Moreover, alloying of Pt with Ce decreases the number of active Pt surface sites for the electrochemical reaction; in this regard, a decrease of hydrogen adsorption by Pt/CeO_2 catalysts due to the formation of Pt–Ce alloy under reducing conditions has been previously reported;[15] this was interpreted in terms of strong metal-support interaction (SMSI) occurring between Pt and ceria.

To summarize, since the main effect on the decrease of cell performance concerns OCV, and having discarded the occurrence of cross-over phenomena and electrical failures, the observed decay can be reasonably explained by a change in the relative composition of reactant gases at the anode, due to a modification of the reaction path towards the deep oxidation to CO_2 and H_2O instead of CO and H_2. This hypothesis is supported by previous studies[10,11] on Pt–ceria catalysts, according to which depletion of CeO_2 together with the presence of zero-valent Ce was reported to shift the selectivity of methane oxidation to the complete oxidation products. In this respect, Bockris and Srinivasan[16] reported that the OCV value of an YSZ solid oxide fuel cell decreased by ~0·3 V passing from an anode feed containing pure CO to a 60% CO–40% CO_2 mixture; moreover, an OCV decrease of 0·4 V was recorded upon dilution of H_2 stream with 50% water.[16] Interestingly, in the latter case no significant mass-transfer limitations at high current densities were observed. In this respect, the anode feed is in our case, significantly in excess if compared to that required by the faradaic reaction in the selected range of current densities. Thus, the change in feed composition did not introduce significant diffusion control.

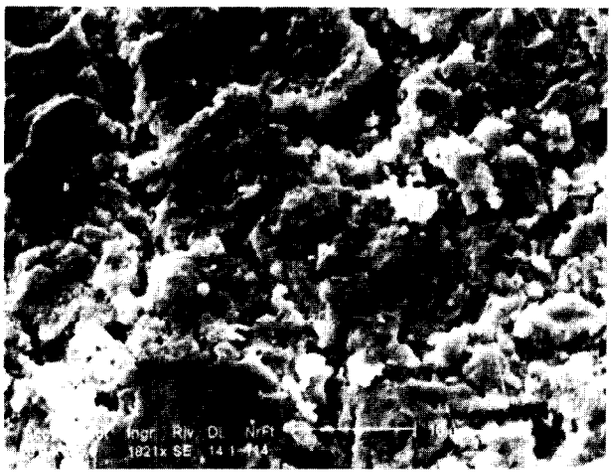

(a)

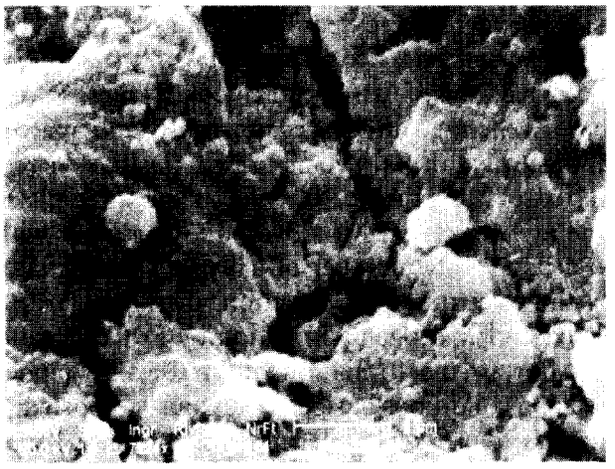

(b)

Fig. 7. Scanning electron micrographs of cell 0 at different magnifications: (a) 1800 ×, (b) 7000 ×.

To definitively confirm the above evidence, a few experiments were carried out on a single cell fed at the anode with synthesis gas containing increasing amounts of inert H_2O and CO_2 species; a progressive decrease of OCV, up to a value of 0·65 V, was correspondingly observed.

No relevant variations in particle size dimension between the reference and aged cells were observed from peak profiles analysis of the anode catalyst. The average particle size was around 300 Å for Pt and 250 Å for CeO_2 It is thought that the strong metal-support interaction between Pt and CeO_2 reduced the sintering effects due to operation at high temperature. This apparent stability could also arise from some redispersion phenomena which are often encountered for Pt-supported catalysts treated in air at temperatures between 400 and 500°C;[17–19] these conditions occur during the shut-down procedure of the stack.

Another remarkable factor is that no evidence of carbon formation was found in any of the examined electrodes; from this it is deduced that the catalytic role of cerium oxide for carbon gasification,[20] even at the low oxidant/fuel ratio adopted, was not significantly affected by the observed ceria depletion.

Scanning electron micrographs [Fig. 7(a) and(b)] of the reference cell showed a continuous matrix with only slight evidence of cracks, resulting in a compact structure. Anodes of cells 6 and 3 [Fig. 8(a) and (b) and Fig. 9(a) and (b), respectively] were characterized by the presence of discontinuities in the layers, with an increased presence of voids and channels. The particles are soldered together in the reference anode, avoiding a clear distinction of grain boundaries. From this evidence, it could be assessed that surface porosity increases for cells 3 and 6; accordingly, a more corrugated morphology is clearly visible. The higher degree of voids in the electrode structure of cell 3 is thought to contribute also to the increased internal resistance of this cell. Further, a clear change in crystallite morphology is observed for the samples subjected to operation temperature for a prolonged time, with the particles having well-defined boundaries [Fig. 8(b) and Fig. 9(b)].

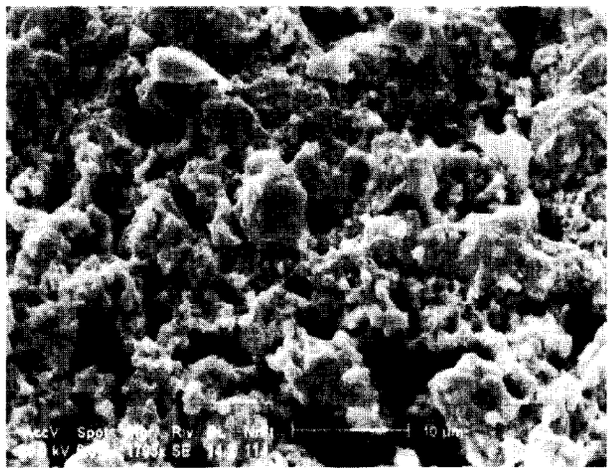

(a)

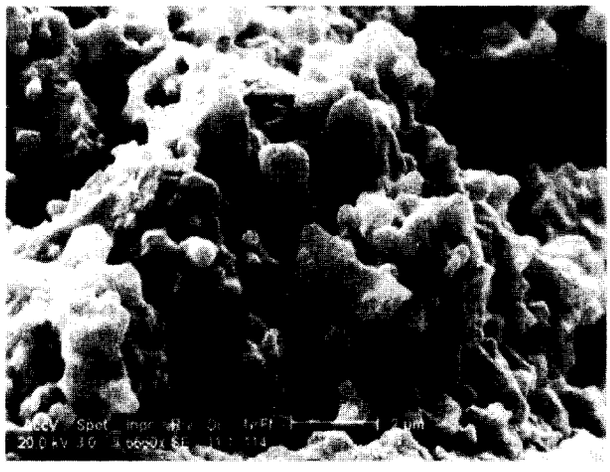

(b)

Fig. 8. Scanning electron micrographs of cell 6 at different magnifications: (a) 1800 ×, (b) 6000 ×.

(a)

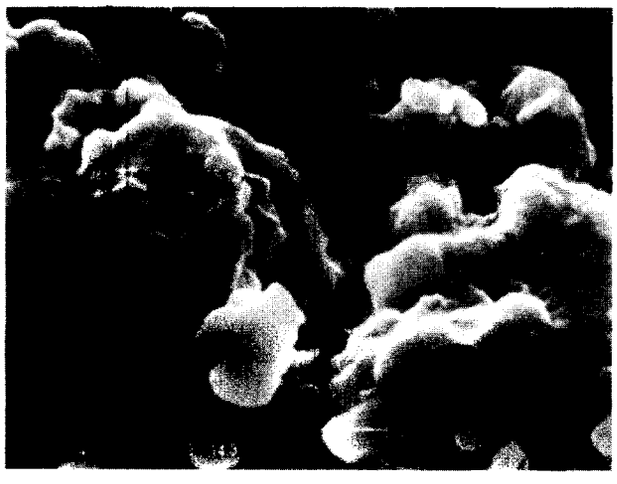

(b)

Fig. 9. Scanning electron micrographs of cell 3 at different magnifications: (a) 900 ×, (b) 7000 ×.

Figure 10(a)–(c) shows the transmission electron micrographs of the anode in the reference and in cell 3, respectively. A platinum metal phase associated with the cerium oxide layer is clearly visible in Fig. 10(a); a non-uniform distribution in Pt particles dimension is also apparent, with Pt size ranging over a rather wide interval (150–300 Å). However, no significant sintering phenomena are evident in the anode of cell 3 [Fig. 10(b)], where Pt particles still appear to be confined in a dimension range not exceeding 300 Å; on the other hand, the presence of ceria is no longer clearly distinguishable from platinum, thus suggesting that a more relevant interaction has interested the two species on account of prolonged operation. A high magnification view of the anode surface [Fig. 10(c)] appears to indicate a very close arrangement of the two lattices, resulting in a parallel epitaxial alignment. Evidence of such behaviour for Pt–CeO_2 interaction has been previously reported in literature,[21–23] and a Pt lattice distortion at the metal–oxide interface was invoked to explain some unusual catalytic properties of Pt-CeO_2 catalysts. Accordingly, after high temperature (>773K) reduction, Pt particles are aligned with ceria, the lattice mismatch between the two phases being accommodated by an array of edge dislocations at the Pt–CeO_2 interface. The mobility of lattice oxygen in ceria, and thus its reducibility when in contact with Pt, was attributed to the nature of the metal–oxide interface.

4.2 Cathodes

Figure 11 shows the XRD patterns of the cathodes under examination. The typical reflections of platinum and praseodymium oxide (card no. 24-1006) are present in the reference cell; the intensity of peaks pertaining to PrO_2 denotes a prevailing presence of the oxide in its cubic form. Further, diffraction peaks at $2\theta = 28{\cdot}3°$ and $55{\cdot}9°$ are indicative of some presence of the sub-stoichiometric $PrO_{1{\cdot}83}$ cubic form. This latter clearly appears to prevail in cells 3 and 6, for which an almost complete disappearance of the stoichiometric oxide is denoted by the absence of related peaks, in comparison with the reference. This accounts for a relevant decrease in the ionic contribution to conductivity.

Moreover, some evidence for the presence of a Pr–Pt alloy phase comes from the reflection at $2\theta = 34{\cdot}4°$ in the used cathodes. However, the most apparent feature resulting from the comparison of the three diffractograms is represented by the net decrease in PrO_2 concentration at the electrode surface. This is further confirmed by EDX [Fig. 12(a)–(c)], according to which the initial Pt–Pr atomic ratio (0·86) changes up to a value of 1·8 in the worst-functioning cell (3).

The observed structural evolution of praseodymia, passing from the stoichiometric to a substoichiometric form with ageing, is explained on the basis of the thermodynamic behaviour exhibited by this oxide at different temperatures, similar to other binary rare earth oxides such as cerium and terbium oxides; accordingly, there exist, in the same region of the phase diagram, ordered stoichiometric phases of a homologous series (general formula: M_nO_{2n-2}) at low temperatures, and a disordered, non-stoichiometric phase at higher temperatures, on account of a short-range order of a kind which also occurs and extends to long range in the ordered phases.[24]

The strong depletion in PrO_2, denoted by EDX, contributes to the activity decay of the stack. As previously stated, the electrochemical activity of gas electrodes in SOFCs can be increased by the introduction (as subsurface electrolyte layer) of oxides with mixed conductivity, such as PrO_2 as in the present case. These oxides (besides PrO_2, rare-earth nickelates and cobaltates, iron-strontium

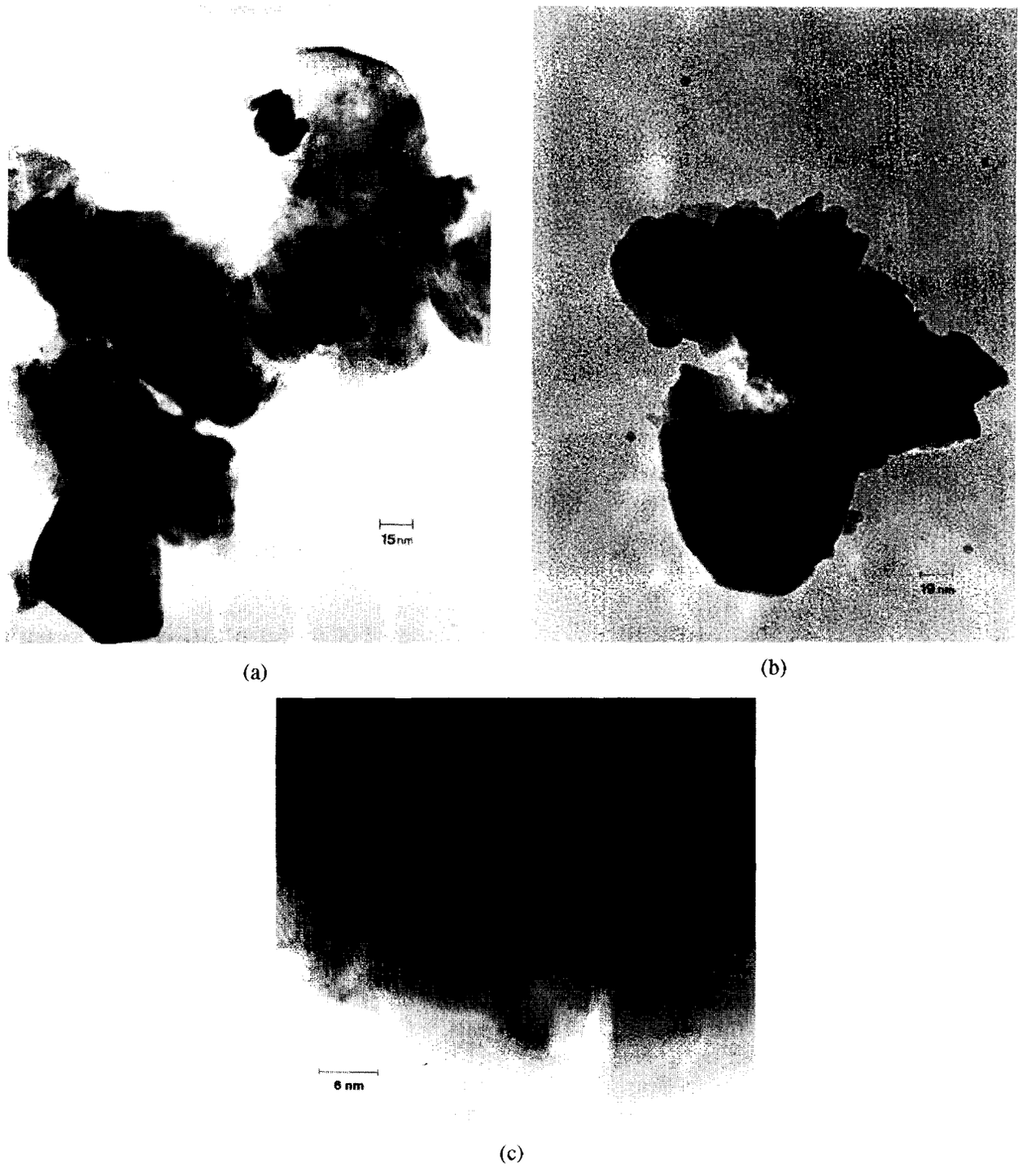

Fig. 10. Transmission electron micrographs of the anode layers: (a) cell 0, (b) cell 3, (c) high magnification micrograph of cell 3.

oxide and other electronically conducting oxides in the perovskite family fulfil the criteria) have sufficient oxygen mobility as well as electronic conduction to facilitate oxygen ionization and transfer into the adjacent electrolyte. Transition from electronic to mixed (ionic + electronic) subsurface conductivity is reflected by a significant decrease in overvoltage. As previously observed for the anode side, such a contribution of mobile electronic defects also results in a widening of the reaction zone around the triple contact point, with consequently increased reaction rates. The higher electrocatalytic activity of the Pt–PrO_2 electrode, in comparison with Pt alone, has been previously demonstrated.[25]

Line-broadening analysis of X-ray diffraction patterns confirms the increase, although not significant, of Pt particle dimension in the aged cells. The mean particle size increases from 250 Å in the reference to 330 Å in the worst-functioning cell. The peak profiles analysis cannot apply for praseodymium oxide, since a phase transition from PrO_2 to $PrO_{1.83}$ occurred during prolonged operation at high temperature. However, such a small

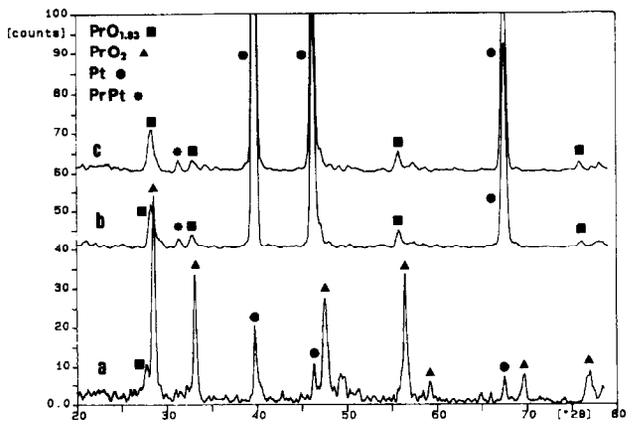

Fig. 11. XRD patterns ofthe cathode layers: (a) cell 0, (b) cell 6, (c) cell 3.

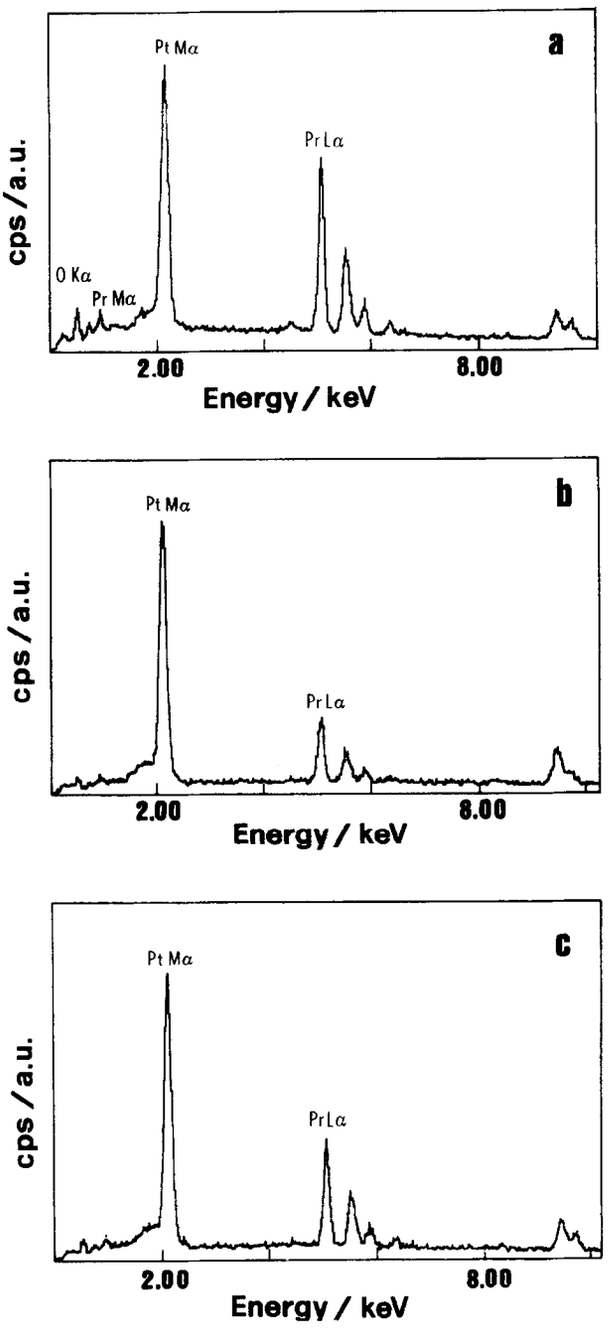

Fig. 12. EDX spectra of the cathode layers: (a) cell 0, (b) cell 6, (c) cell 3.

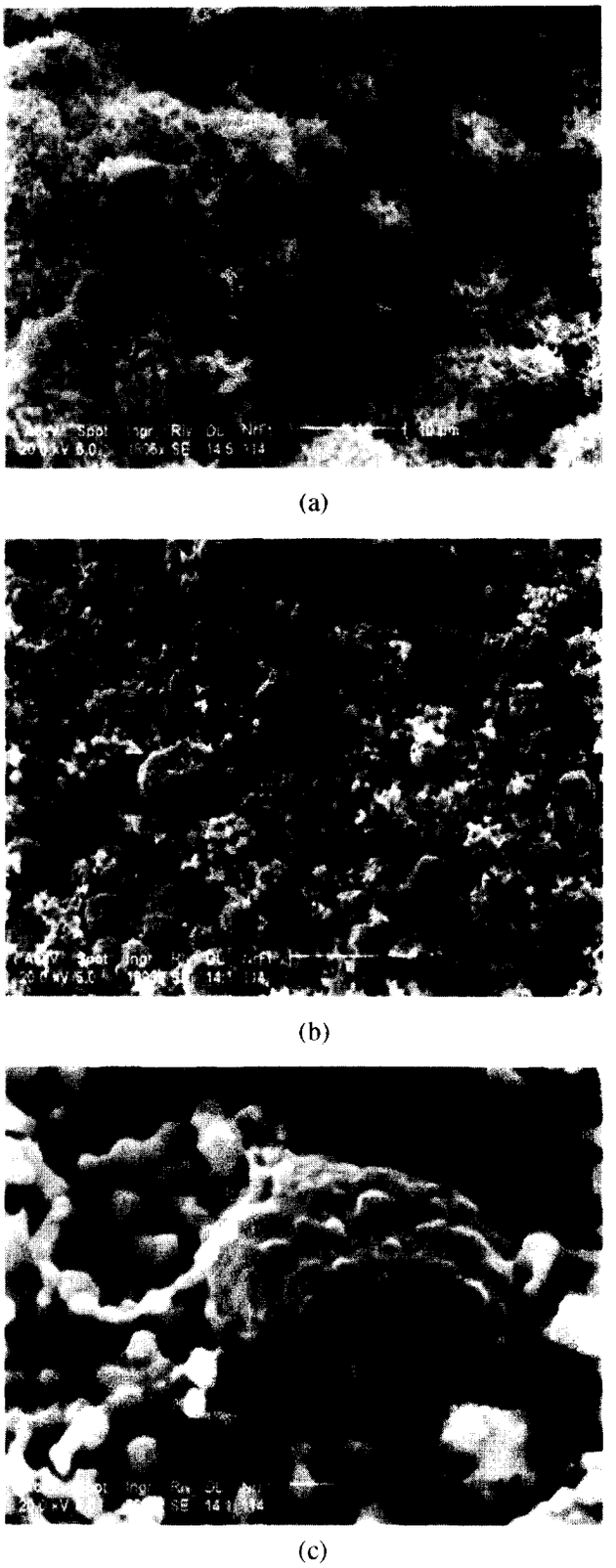

(a)

(b)

(c)

Fig. 13. Scanning electron micrographs of the cathodes: (a) cell 0, (b) cell 3, (c) cell 3, 7600 ×.

increase in Pt dimension is not easily explainable without taking into account some redispersion effects, also invoked for the anode catalyst, which probably occurred during shut-down cycles.

Examination of SEM micrographs yields more information on the morphological evolution of the

electrodes on account of stack operation; Fig. 13(a) is illustrative of the distribution of Pr oxide particles over the continuous platinum layer. The image of Fig. 13(b) (sample 3) shows Pt agglomerates (dimension: 3–10 μm) around which the Pr oxide phase also appears to be interested to sintering phenomena; Fig. 13(c) clearly depicts the morphological arrangement of catalyst particles consequent to stack operation.

5 Conclusions

The above reported physico-chemical characterization of electrode components of an SOFC stack, made after a 3000 h endurance test, has allowed identification of most of the factors that have determined its performance decay. Significant modifications occurred at the anode, consisting of the depletion of CeO_2 and formation of a Pt–Ce alloy, resulting in a substantial change of the reaction path, leading to the complete oxidation products. Accordingly, the lower H_2–CO partial pressure gave rise to the OCV drop, resulting in the observed performance decay. In addition, removal of praseodymia from the cathode surface and formation of Pt–Pr alloy forced the original mixed conduction characteristics at the electrode–electrolyte interface to fail, with an increase in interfacial resistance.

References

1. Minh, N. Q., Ceramic fuel cell. *J. Am. Ceram. Soc.*, 1993, **76** (3), 563–588.
2. Badwal, S. P. S. and Foger, K., Solid electrolyte fuel cell review. *Ceram. International*, 1966, **22**, 257–265.
3. Subbarao, E. C. and Maiti, H. S., Solid electrolyte with oxygen ion conduction. *Solid State Ionics*, 1984, **11**, 317–338.
4. Feduska, W. and Isemberg, A. O., High temperature solid oxide fuel cell—technical status. *J. Power Sources*, 1983, **10**, 89–102.
5. Hirschenhofer, J. H., Stauffer, D. B., Engleman, R. R., Solid oxide fuel cell. In *Fuel cells, A Handbook (Revision 3)*, Vol 5. DOE/METC-94/1006, US Department of Energy, Hargentown, **5**, 1994, pp. 1–26.
6. Antonucci, V., Antonucci, P. L., Aricò, A. S. and Giordano, N., Partial oxidation of methane in solid oxide fuel cells: an experimental evaluation. *J. Power Sources*, 1996, **62**, 95–99.
7. Antonucci, V., Natural Gas Reforming. In *Small SOFC Units, Proceedings of 1st. European Solid Oxide Fuel Cell Forum*, ed. U. Bossel. Lucerne, 1994, pp. 183–195.
8. Antonucci, V., Antonucci, P. L., Aricò, A. S., Arato, E., Costamagna, P., Rocchini, G. and Demin, A., Partial oxidation of CH_4 for SOFC: performance analysis. In *Solid Oxide Fuel Cell IV*, ed. M. Dokya, O. Yamamoto, H. Tagawa and S. C. Singhal. The Electrochemical Soc., Pennington, USA. 1995, pp. 820–828.
9. Otsuka, K., Ushiyama, T. and Yamanaka, I., Partial oxidation of methane using the redox of cerium oxide. *Chem. Letters*, 1993, pp. 1517–1520.
10. Trovarelli, A., Catalytic properties of ceria and CeO_2-containing materials. *Cat. Rev.—Sci. Eng.*, 1996, **38**(4), 439–520.
11. Oh, S. H., Mitchell, P. J. and Siewert, R. M., Methane oxidation over alumina-supported noble metal catalysts with and without cerium additives. *J. Catal*, 1991, **132**, 287–301.
12. Schouler, E. J. L. and Kleitz, M., Electrocatalysis and inductive effects at the gas, Pt/stabilized zirconia interface. *Journal of Electrochemical Society*, 1987, **134**(5), 1045–1050.
13. Isemberg, A. O., Energy conversion via solid oxide electrolyte electrochemical cells at high temperatures. *Solid State Ionics*, 1981, **3/4**, 431–437. Elsevier, Amsterdam.
14. Sunde, S., Monte Carlo simulations of polarization resistance of composite electrodes for solid oxide fuel cells. *Journal of Electrochemical Society*, 1996, **143**(6), 1930–1939.
15. Meriaudeau, P., Dutel, J. F., Dufaux, M. and Naccache, C., Further investigation on metal-support interaction: TiO_2, CeO_2, SiO_2 supported platinum catalysts. In *Metal-Support and Metal-Additive Effects in Catalysis*, ed. B. Imelik. 1982, pp. 95–103.
16. Bockris, J. O'M. and Srinivasan, S. In *Fuel Cells: Their Electrochemistry*, McGraw-Hill, New York. 1969, pp. 585–588.
17. Straguzzi, G. I., Aduriz, H. R. and Gigola, C. E., Redispersion of platinum on alumina support. *J. Catal.*, 1980, **66**, 171–183.
18. Guo, I., Yu, T. T. and Wanke, S. E., Changes in Pt crystallite sizes as a result of treating Pt/Al_2O_3 catalysts in different atmospheres. In *Catalysis*, ed. J. W. Ward, 1987, pp. 21–32. Elsevier, Amsterdam.
19. Dautzenberg, F. M. and Wolters, H. B. M., State of dispersion of platinum in alumina-supported catalysts. *J. Catal.*, 1978, **51**, 26–39.
20. Mckee, D. W., Rare earth oxides as carbon oxidation catalysts. *Carbon.*, 1985, **23**(6), 707–713.
21. Hardacre, C., Rayment, T. and Lambert, R. M., Platinum/ceria CO oxidation derived from Pt/Ce crystalline alloy precursor. *J. Catal.*, 1996, **158**, 102–108.
22. Kalakkad, D. S., Datye, A. K. and Robota, H. J., Pt-CeO_2 contact and its effect on CO hydrogenation selectivity. *J. Catal.*, 1994, **148**, 729–736.
23. Datye, A. K., Kalakkad, D. S., Yao, M. H. and Smith, D. J., Comparison of metal-support interactions Pt/TiO_2 and Pt/CeO_2. *Catal.*, 1995, **155**, 148–153.
24. Bevan, D. J. M., Non-stoichiometric compounds. In *Comprehensive Inorganic Chemistry*, Vol. 4, ed. J. C. Bailar, H. J. Emeléus, Sir Ronald Nyholm and A. F. Trotman-Dickenson, 1973, pp. 453–540. Pergamon Press, Oxford.
25. Kuzin, B. L., Demin, A. K. and Komarova, N. Y., Electrochemical behaviour of $Pt + PrO_{2-x}$-oxygen electrode in contact with solid oxide electrolyte. *Electrochimia (rus)*, 1984, **20**(12), 1636–1642.